Direct imaging of tunnel cations in zinkenite by high-resolution electron microscopy

PIERS P. K. SMITH

Research School of Chemistry
Australian National University
G.P.O. Box 4, Canberra, A.C.T. 2601, Australia

Abstract

The metal atoms in a sample of zinkenite from Wolfsberg, Germany, have been imaged directly by high-resolution transmission electron microscopy (HREM). The [001] image shows that the tunnel cation sites on the sixfold screw axes are at least partially occupied; previous studies have given conflicting results concerning the occupancy of these sites. Dark-field electron micrographs and [010] high-resolution images show that zinkenite has a domain structure; the average hexagonal structure consists of ordered domains with orthorhombic lattice geometry. The domains are in three orientations and have a rodlike morphology extending parallel to **c**.

Introduction

The crystal structure of the sulfosalt zinkenite, approximate formula $Pb_6Sb_{14}S_{27}$, was determined by Takeda and Horiuchi (1971) and has subsequently been refined by Portheine and Nowacki (1975) and Lebas and Le Bihan (1976). A notable feature of the zinkenite structure (Fig. 1) is the relatively large cation site on the sixfold screw axis, forming a tunnel along the **c** axis, and the two X-ray refinements differ markedly in the reported occupancies of these tunnel sites. Whereas Portheine and Nowacki (1975) found a total occupancy of 0.74 Pb atoms per 4.3 Å pseudorepeat along the **c** axis, Lebas and Le Bihan (1976) found the tunnels to be empty. The present paper describes an attempt to resolve this discrepancy by using high-resolution electron microscopy (HREM) to image the tunnel contents. Also, dark-field electron microscopy has been used to elucidate the ordered superstructure of zinkenite and to show that the ordering results in a domain structure.

Vaux and Bannister (1938) showed that zinkenite has hexagonal symmetry, space group $P6_3$ or $P6_3/m$, with $a = 44.06$, $c = 8.60$ Å; a prominent subcell was noted with half these axial dimensions. The superlattice reflections were diffuse, indicating some degree of disorder. The two structure refinements mentioned above confirm the existence of a superlattice, although Portheine and Nowacki (1975) found the ordering to be restricted to the z direction. Both X-ray refinements confirmed $P6_3$ as the correct space group for the average structure, although the departures from centrosymmetric $P6_3/m$ symmetry are only minor.

The backbone of the zinkenite structure (Fig. 1) is a triangular beam formed by three edge-sharing PbS_6 trigonal prisms located around the 3-fold axis. The prisms are each capped on two square faces to give 8-fold coordination of the lead atoms by sulfur. This triangular beam is a distinctive structural motif in many sulfosalts, for example the Sn,Sb sulfosalts described by Smith (1985). In zinkenite the triangular beams are linked across the screw diad axes by slabs containing octahedrally-coordinated antimony atoms in rather distorted $B1$ structure. A ring of MS_6 trigonal prisms around the 6_3 axis, each capped by sulfur atoms of two adjacent prisms, completes the structural framework. Portheine and Nowacki (1975) found this site to be occupied equally by Pb and Sb on a statistical basis; Lebas and Le Bihan (1976) reported it to be occupied solely by Sb.

The other available cation position is the 9-coordinated site on the 6_3 axis at 0,0,0.25 (subcell). This site is a trigonal prism formed by three sulfurs at $z = 0.75$ and three at $z = -0.25$, capped by three further sulfurs at the same height as the cation. Portheine and Nowacki (1975) located Pb atoms at 0,0,0.125 and 0,0,0.365 with occupancies 0.18 and 0.19, respectively; these atoms are thus displaced from the center of the trigonal prism. It is clear that this off-center displacement and the possibility of occupying prisms centered at either $z = 0.25$ or $z = 0.75$ may both lead to ordering along the z direction. As mentioned above, Lebas and Le Bihan (1976) found no electron density on the 6-fold screw axis, leaving an empty tunnel of diameter 5.1 Å between opposite sulfur atoms in the [001] projection.

Recent work by Smith and Parise (1985) shows that the metal atoms in sulfosalts can be located directly in HREM images taken along the short (~4 Å) crystallographic repeat axis. HREM should thus be able to distinguish between the empty-tunnel and occupied-tunnel structures previously described for zinkenite. It should be recognized at the outset that the tunnel contents may differ from sample to sample, although the range reported (zero to 0.74 Pb per subcell) seems unlikely on crystal chemical grounds.
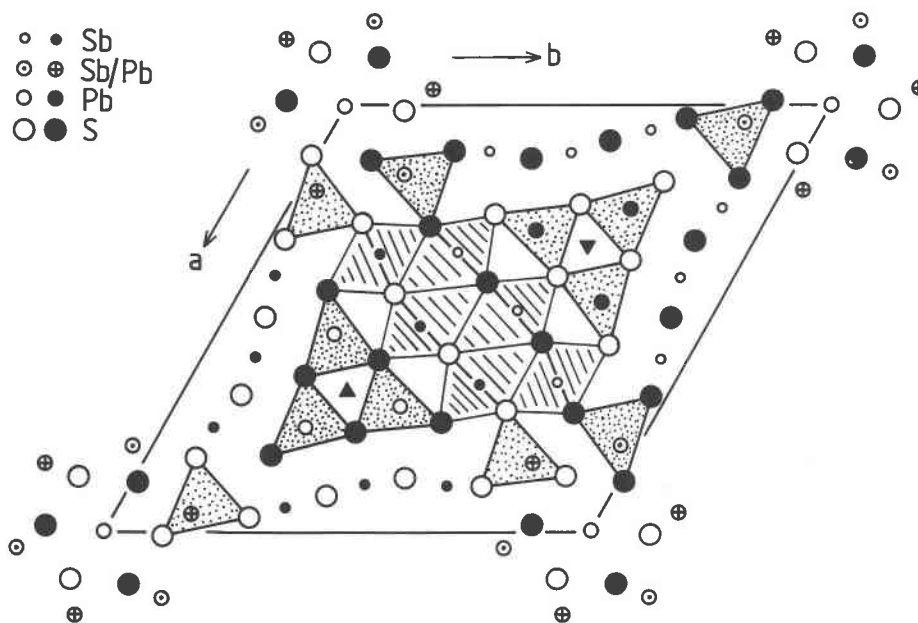
Fig. 1. The structure of zinkenite projected on (001). Open symbols have $z \approx 0.25$, filled symbols $z \approx 0.75$. Trigonal prisms are dot shaded, octahedra line shaded. The occupancy of the $0,0,z$ site on the 6-fold axis is discussed in the text.

Experimental

The material examined was from the type locality at Wolfsberg in the Harz Mountains, Germany. Least squares refinement of the subcell dimensions from X-ray powder diffraction data gives $a = 22.108(2)$, $c = 4.3265(4)$ Å (Guinier camera, CuKα_1 radiation, Si standard N.B.S. 640a, cell refined from 15 reflections in the range $28° < 2\theta < 64°$). The sample was analyzed for Pb, Sb and S with a Cameca electron microprobe operating at 15kV; natural galena and stibnite were used as standards. The mean composition from ten spots is Pb(0.1219) Sb(0.3060) S(0.5721) (Table 1). This corresponds to a Pb/Sb ratio of 0.398(2), significantly lower than the value 0.429 required by the generally accepted formula $Pb_6Sb_{14}S_{27}$. Possible reasons for this discrepancy will be discussed later.

An initial electron diffraction study and the dark-field imaging described below were performed with a JEOL 100CX 100 kV electron microscope equipped with a tilt ($\pm 60°$)-rotate specimen holder. The sample was crushed in an agate mortar and dispersed on a holey-carbon support film. The [010] electron diffraction pattern (Fig. 2) confirms the existence of a superlattice with doubled a and c dimensions as first described by Vaux and Bannister (1938). The superlattice reflections are somewhat streaked along

Table 1. Electron microprobe analysis of Wolfsberg zinkenite. Mean of ten spots, range given in parentheses

	Weight percent	atom proportion
Pb	31.01 (30.77-31.17)	0.1219
Sb	45.75 (45.34-46.02)	0.3060
S	22.53 (22.38-22.69)	0.5721
Total	99.29 (98.71-99.64)	1.0000

a^*. This superlattice has also been observed in the [1$\bar{1}$2], [0$\bar{1}$2] and [0$\bar{1}$1] (subcell) electron diffraction patterns. When indexed according to the $2a,2c$ supercell, the superstructure reflections are only present on the $l = 2n + 1$ layers of the reciprocal lattice, and they also display the systematic absences $h0l$, $h + l = 2n + 1$ and $0kl$, $k + l = 2n + 1$. This reciprocal lattice does not correspond to a single hexagonal space group, and it will become clear that the apparent hexagonal superlattice results from twinning of a structure of lower symmetry. For the moment we may note that no ordering reflections occur in the $hk0$ plane ($l = 2n$), thus structure images in the [001] projection will provide information concerning only the average structure.

[001] Imaging

High-resolution [001] images were obtained with a JEOL 200CX electron microscope operating at 200 kV, equipped with a high-resolution objective lens pole-piece ($C_s = 1.2$ mm) and a double-tilt ($\pm 10°$) specimen holder. Since suitable cleavage fragments close to (001) could not be obtained by crushing, samples were prepared by ion-beam thinning of a thin section cut perpendicular to the needle axis [001]. Samples were thinned to perforation at a gun voltage of 3.5 kV, then thinned for a further 2–3 hours at 1.5 kV to reduce specimen damage.

Images were recorded from the thin edge of the sample at a small negative defocus of the objective lens. Lynch et al. (1975) have shown that under these conditions experimental images of a sufficiently thin crystal correspond to the projected charge density (PCD) of the crystal structure, up to a maximum defocus given approximately by the Scherzer value $-1.2\sqrt{C_s\lambda}$ (-660 Å). Within this focus range the rate of change of the image character is at a minimum, with the overall contrast increasing with increasing defocus. An [001] image recorded at an electron optical magnification of 810000 is shown in Figure 3. The corresponding [001] electron diffraction pattern (Fig. 4) shows weak superlattice reflections at {1/3,1/3,0}; however these are only observed for
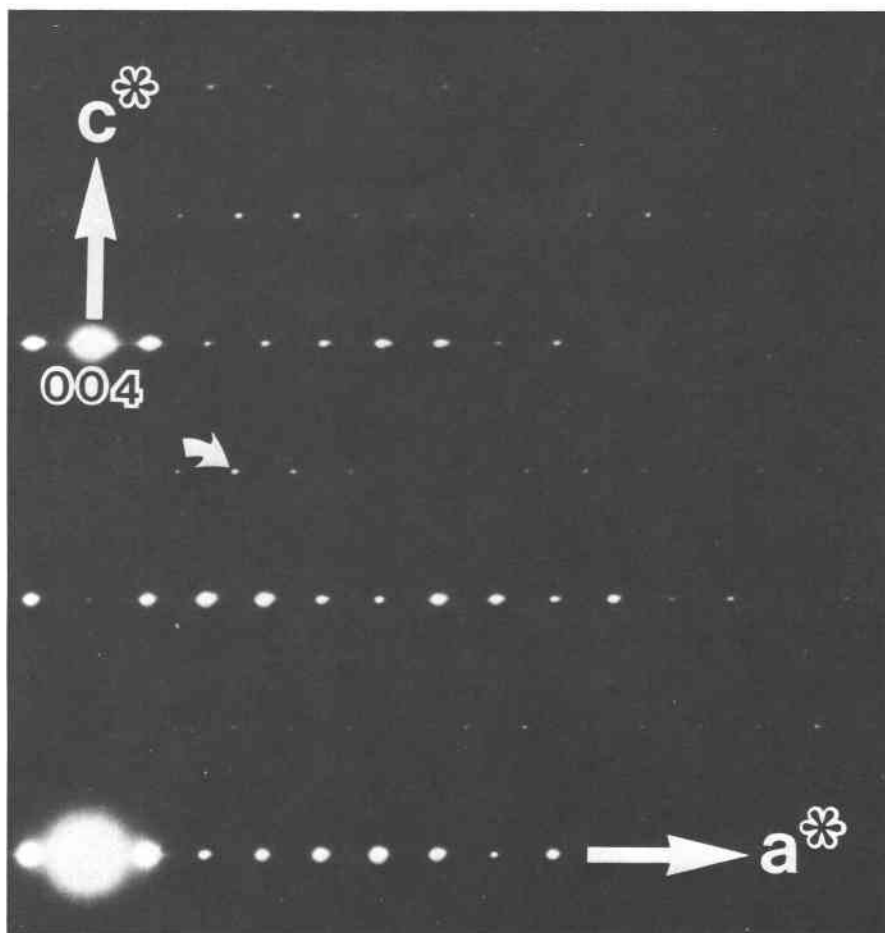
Fig. 2.   The [010] electron diffraction pattern of zinkenite. Superlattice reflections occur on alternate rows, e.g., the 503 reflection arrowed. Streaking of reflections along **a*** is seen best around the 004 reflection.

ion-thinned samples (not crushed samples) and must therefore be an artefact.

Simulated HREM images (Fig. 5) were computed by means of the multislice method (Cowley and Moodie, 1957), using a suite of programs written by G. R. Anstis (New South Wales Institute of Technology). The multislice iteration is performed with the algorithm of Ishizuka and Uyeda (1977). Images were calculated for three models based on Portheine and Nowacki's (1975) structure refinement: (a) tunnels empty, (b) tunnel contents as published, i.e., 0.74 Pb per subcell, (c) maximum tunnel occupancy of 1.0 Pb. A crystal thickness of 20 Å was assumed as this value gave good agreement between experimental and calculated images of ion-thinned $SnSb_2S_4$ (Smith and Parise, 1985); however, images vary only slightly for thicknesses up to 50 Å. Experimentally determined values of 0.77 $Å^{-1}$ and 1.6 mrad were used for the objective aperture radius and beam divergence; a value of 50 Å was assumed for the halfwidth of focus (chromatic aberration). Images were calculated for defocus values of −350, −500 and −650 Å.

As anticipated from the PCD approximation, the calculated images differ only slightly for the different focus settings, and the images for the three models differ only at the tunnel site. Notice that models (b) and (c) can be distinguished by the intensity of the dark spot at the unit cell origin, which depends on the oc-

cupancy of this site. Comparison of the experimental image (Fig. 3) with the calculated images indicates that the experimental defocus is approximately −350 Å. The cations are clearly resolved in the high-resolution image (cf. Fig. 1), and it is clear that the tunnels in the Wolfsberg zinkenite are not empty. There is some variation in contrast across the image, probably as a result of ion-beam or electron-beam damage, but the image intensity at the tunnel position is generally less dark than the surrounding cation sites in accordance with model (b). The high-resolution [001] image is thus consistent with the zinkenite structure published by Portheine and Nowacki (1975).

Domain structure

The doubled c cell dimension indicates the existence of a superstructure along this direction, and it seems likely that this is due to ordering of the mixed Pb/Sb site M(4) adjacent to the tunnels, possibly with an associated ordering of the tunnel cations. The ordering along **a** then implies some degree of correlation between adjacent tunnels. The simplest way to account for the doubled a and c dimensions is to form a "face-centered hexagonal" superlattice as in Figure 6. This ordering scheme destroys the hexagonal symmetry, and the superlattice may be de-
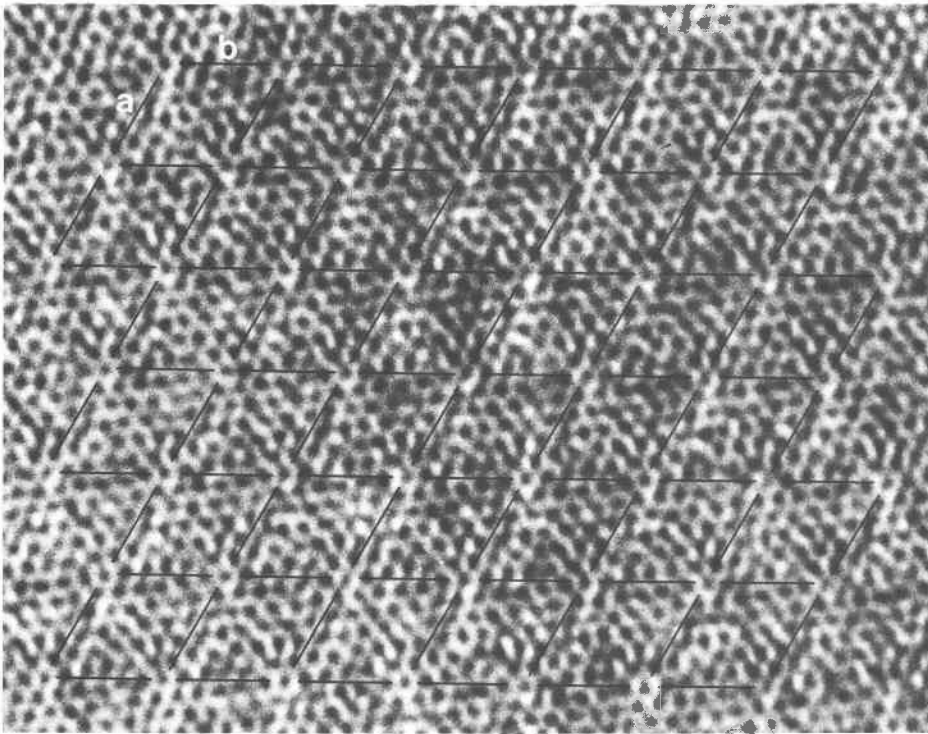
Fig. 3. High-resolution [001] image of zinkenite with the unit-cells outlined to aid interpretation. Dark spots in the image correspond to cation positions in the crystal structure; notice the atom at the origin of each cell. Scale: $a = b = 22.1$ Å.
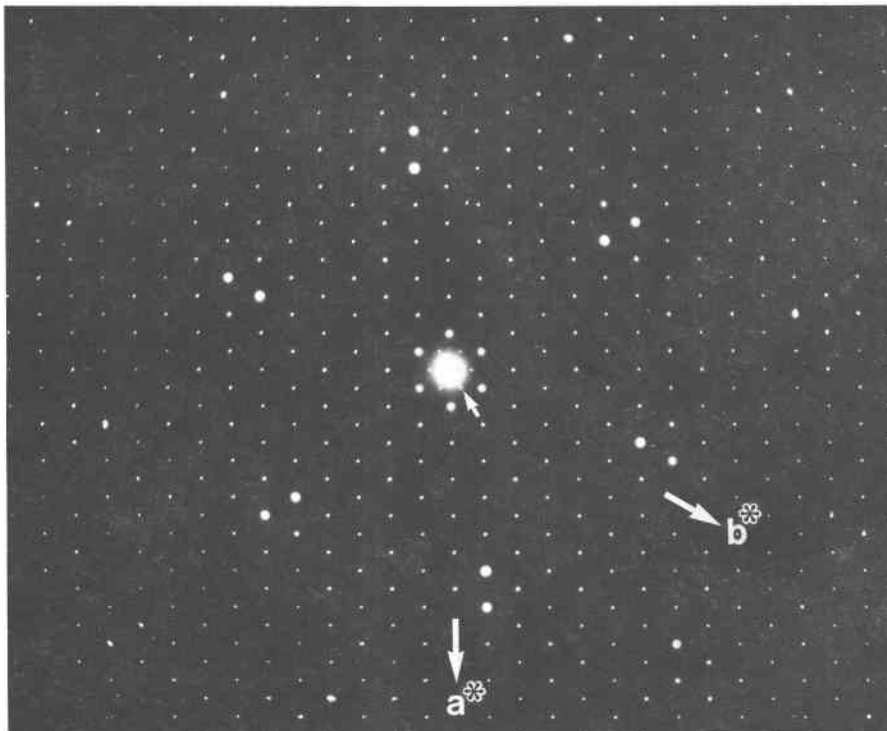

Fig. 4. [001] electron diffraction pattern of ion-beam thinned zinkenite. The weak superlattice reflections (arrowed) are not observed for samples prepared by crushing.
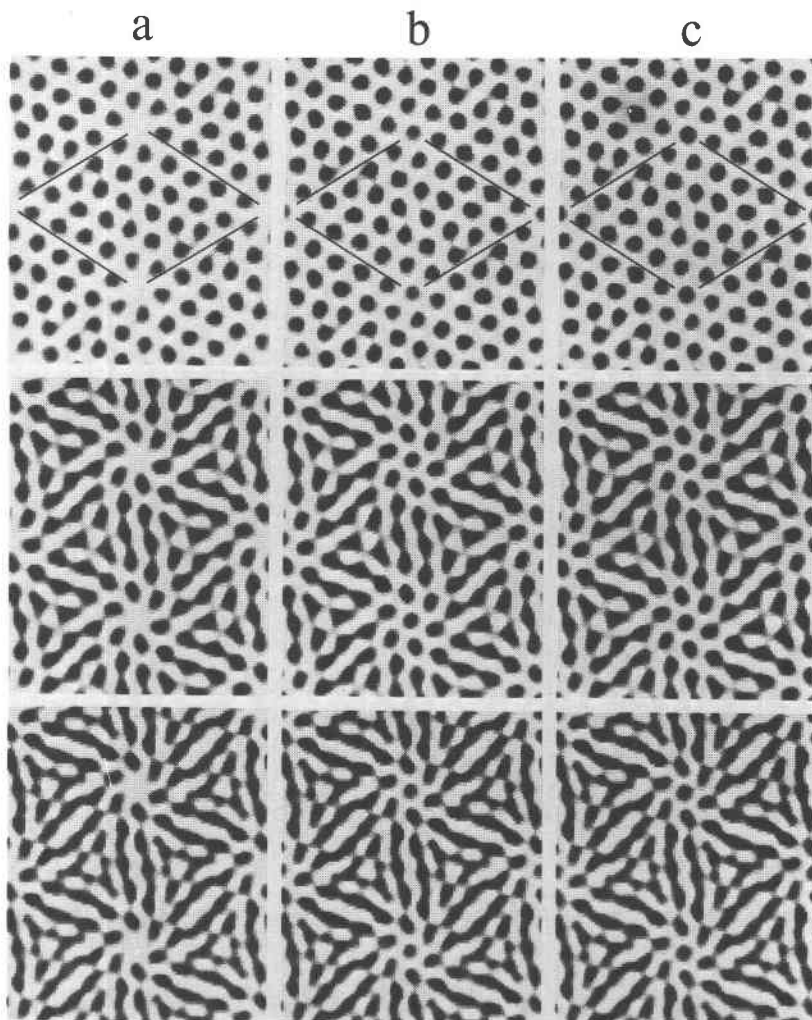
a   b   c

Fig. 5.   Computed [001] images for three zinkenite models: (a) vacant tunnels, (b) partially-filled tunnels, (c) filled tunnels. Defocus −350 Å (top), −500 Å (center), −650 Å (bottom).

scribed by a body-centered orthorhombic unit cell with dimensions $|a'| = |a\sqrt{3}|$, $|b'| = |a|$, $|c'| = |2c|$. Although this cell has orthorhombic lattice geometry, the space group symmetry of the superlattice is $P1$, as the 6_3, 3 and 2_1 rotation axes of $P6_3$ are all destroyed by the ordering process.

It should be noted that the doubling of the a and c dimensions requires that the lattice symmetry be reduced from hexagonal to orthorhombic. It is thus apparent that a domain structure must result, as the orthorhombic cell may be taken in three orientations with $\mathbf{a}'$ parallel to $[1\bar{1}0]$, [210] or [120]. The hexagonal symmetry observed in single-crystal X-ray and electron diffraction patterns results from superposition of diffraction patterns from the three possible domain orientations. Since the electron diffraction patterns were obtained from areas ~0.5 μm across, the domains must be on a finer scale than this.

Dark-field electron microscopy was used to investigate the predicted domain structure. In a dark-field image formed with one of the superlattice reflections, only those domains contributing to the particular reflection will ap-

pear bright. Figure 7 is an image formed with the 511 reflection of the superlattice (as indexed on the pseudo-hexagonal cell), the crystal being oriented with the electron beam parallel to $[0\bar{1}1]$. The superlattice reflections are
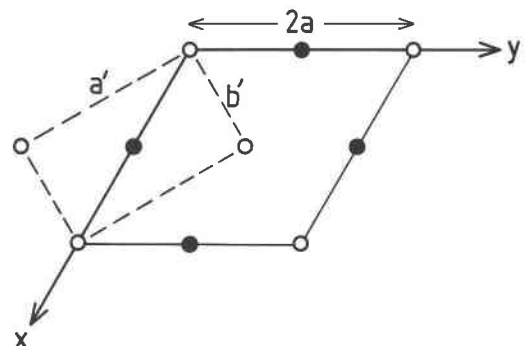

Fig. 6.   Schematic diagram of the proposed zinkenite superlattice. Open circles represent lattice points at $z = 0$, filled circles are the face-center lattice points at $z = 0.5$. The resulting body-centered orthorhombic cell ($\mathbf{a}'$,$\mathbf{b}'$) is outlined.
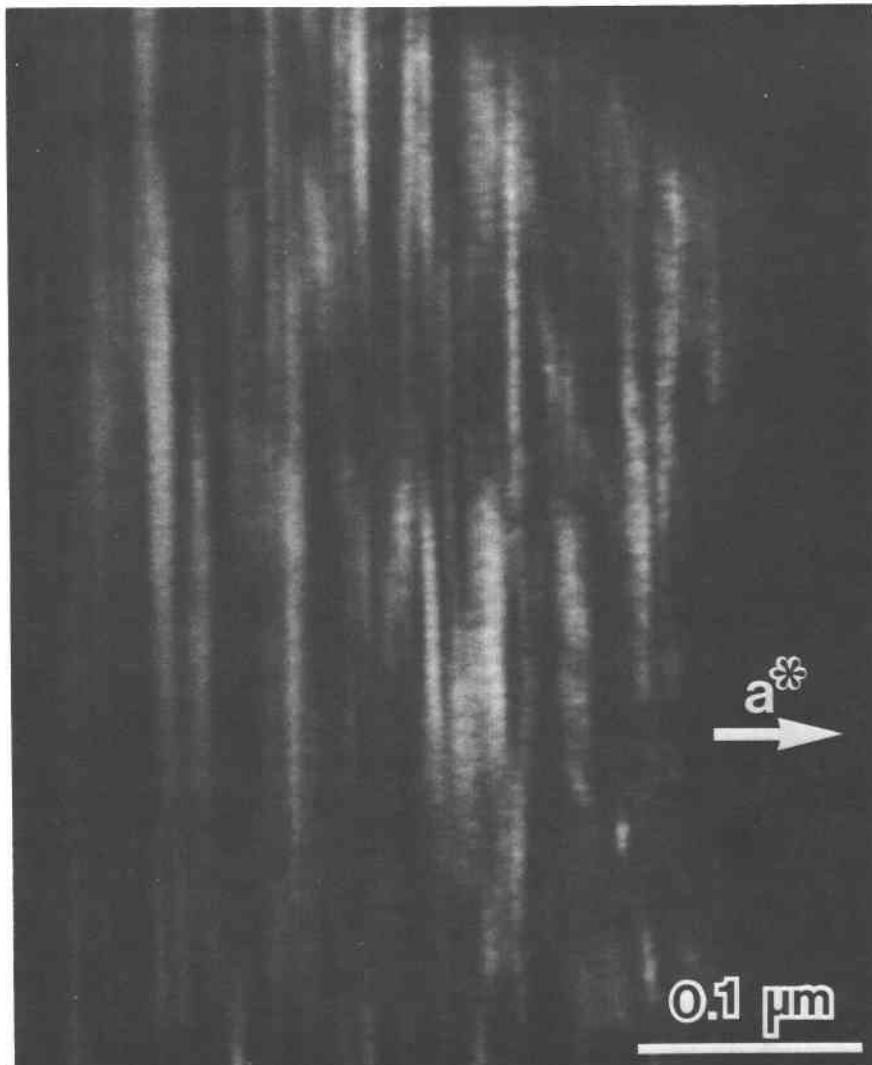
Fig. 7. Dark-field electron micrograph of zinkenite taken with the 511 superlattice reflection.

very weak relative to those from the subcell, necessitating exposure times of 64 s at a magnification of 66000. The dark-field image shows that zinkenite has a domain structure; the elongation of the domain contrast perpendicular to $\mathbf{a}^*$ in the [0$\bar{1}$1] image is consistent with a model having rodlike domains parallel to $\mathbf{c}$. The image contrast is complex, presumably due to the overlap of domains at different depths in the thin foil. The domains are on the order of 100 Å in width; terminations of domains along $\mathbf{c}$ are not seen, indicating lengths of $\sim$0.5 μm or more.

The superlattice has also been investigated by high-resolution imaging along [010]. Figure 8 shows a [010] image of a crushed sample taken with the 200cx microscope; operating conditions were the same as for the [001] image. Since the repeat distance along the beam axis is large (22.1 Å for the subcell), direct interpretation of the image in terms of the structure is not possible. However, the image does confirm the existence of the superlattice and domain structure described above. The area at the right of Figure 8 shows the $c \times a\sqrt{3}/2$ subcell, whereas

in the left part of the image the $2c \times a\sqrt{3}$ centered supercell is evident. This variation in the image can be explained on the basis of the domain structure: of the three possible domain orientations only one will show the superlattice when projected along [010] of the subcell. For example, the orthorhombic supercell in Figure 6 will display the supercell when projected along [110], but it will appear disordered when projected on [100] or [010] (subcell directions). Thus, Figure 8 can be interpreted as two adjacent ordered domains, of which only the left one is oriented to show the superstructure. The scale of the domain structure in the high-resolution image is consistent with that determined by dark-field imaging.

Discussion

The HREM observations demonstrate that the tunnels in the zinkenite structure are at least partially occupied, consistent with Portheine and Nowacki's (1975) refinement of the average structure. The present study demonstrates that in favorable circumstances HREM can be
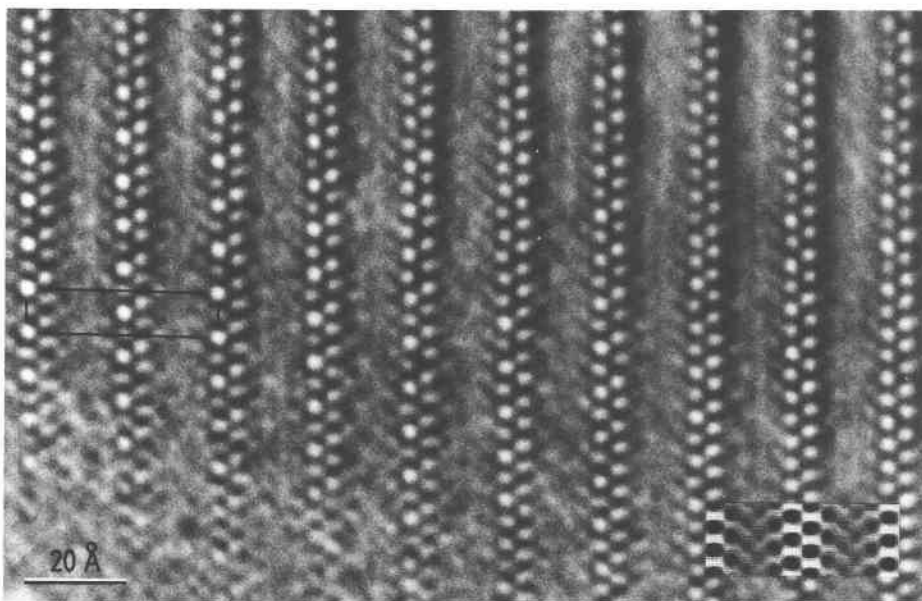
Fig. 8. High-resolution [010] image of a crushed zinkenite sample with the supercell outlined at left. The right-hand part of the image appears disordered; the inset is a computed image assuming the average (Portheine and Nowacki) subcell structure, thickness 40 Å, defocus −450 Å.

used to do "real space crystallography," to obtain information concerning the occupancy of specific atom sites. The dark-field image confirms that zinkenite has a domain structure as first suggested by Lebas and Le Bihan (1976), with rodlike domains parallel to c consistent with the intensity distribution in reciprocal space. Clearly it would be of interest to examine zinkenite samples from other localities by electron microscopy, in order to check for possible variations in the tunnel contents and the scale and morphology of the domain structure.

The microprobe analyses obtained in the present study suggest that reconsideration of the generally accepted formula $Pb_6Sb_{14}S_{27}$ (Pb/Sb = 0.429) may be warranted. This formula was proposed by Vaux and Bannister (1938) on the basis of five previously published analyses; however three of these contain appreciable Cu, possibly as impurities, and the other two give lower Pb/Sb ratios of 0.392 and 0.373. An X-ray spectrographic analysis by Harris (1965) of two samples from Wolfsberg gave Pb:Sb = 6:14 exactly, but sulfur was not determined. Two microprobe analyses of Wolfsberg material by Portheine and Nowacki (1975) give Pb/Sb values of 0.448 and 0.439, but these analyses give poor valency summations.

The formula $Pb_6Sb_{14}S_{27}$ is difficult to reconcile with the crystal structure of zinkenite for the following two reasons. First, if we assume this formula, the subcell content of 42 S atoms implies a total of 31.11 cations per subcell; this in turn requires that 1.11 cations occupy the tunnel sites, as there are only 30 other cation sites available. As pointed out by Portheine and Nowacki (1975), a tunnel occupancy greater than 1.0 per subcell leads to unreasonably close metal–metal distances. These authors overcame this prob-

lem by arbitrarily reducing the occupancy of one sulfur position to accord with the assumed stoichiometry. The second argument is based on density considerations: the 6:14:27 formula with 42 S atoms per subcell gives a calculated density of 5.38, slightly greater than the measured values of 5.33 (Berman, reported in Palache et al., 1944, p. 476), 5.36 (Nuffield, 1946) and 5.28±0.05 (Lebas and Le Bihan, 1976).

These difficulties may be alleviated by reducing the Pb/Sb ratio and also therefore the metal/sulfur ratio. For example, the formula $Pb_9Sb_{22}S_{42}$ or $M_{31}S_{42}$ corresponds to the maximum possible occupancy of the tunnel sites and leads to a calculated density of 5.34. This formula gives Pb/Sb = 0.409, which is close to the value of 0.398 obtained in the present study (Table 1). Partial rather than full occupancy of the tunnel sites would require Pb/Sb < 0.409, assuming 42 S atoms per subcell. It is interesting to note here that Salanci (1979) reported a Pb/Sb solid solution range of 0.377–0.401 for synthetic zinkenites, significantly lower than that required by the 6:14:27 formula. In the light of these observations it is clear that further analyses of natural samples are required in order to establish the compositional range of zinkenite.

Acknowledgments

References

Cowley, J. M. and Moodie, A. F. (1957) The scattering of electrons by atoms and crystals. I. A new theoretical approach. Acta Crystallographica, 10, 609–619.

Harris, D. C. (1965) Zinckenite. Canadian Mineralogist, 8, 381–382.

Ishizuka, K. and Uyeda, N. (1977) A new theoretical and practical approach to the multislice method. Acta Crystallographica, A33, 740–749.

Lebas, Geneviève and Le Bihan, M.-T. (1976) Étude chimique et structurale d'un sulfure naturel: la zinckénite. Bulletin de la Société Française de Minéralogie et Cristallographie, 99, 351–360.

Lynch, D. F., Moodie, A. F., and O'Keefe, M. A. (1975) n-Beam lattice images. V. The use of the charge-density approximation in the interpretation of lattice images. Acta Crystallographica, A31, 300–307.

Nuffield, E. W. (1946) Studies of mineral sulphosalts. XII. Fülöppite and zinckenite. University of Toronto Studies, Geological Series, 50, 49–62 (not seen; extracted from Mineralogical Abstracts, 10, 15–16).

Palache, Clifford, Berman, Harry, and Frondel, Clifford (1944) The System of Mineralogy, Volume I, Seventh Edition. John Wiley and Sons, New York.

Portheine, J. C. and Nowacki, Werner (1975) Refinement of the crystal structure of zinckenite $Pb_6Sb_{14}S_{27}$. Zeitschrift für Kristallographie, 141, 79–96.

Salanci, Berkin (1979) Contribution to the system $PbS–Sb_2S_3$ in relation to lead-antimony sulfosalts. Neues Jahrbuch für Mineralogie Abhandlungen, 135, 315–326.

Smith, P. P. K. (1985) Crystal structure relationships in the system $SnS–Sb_2S_3$. Journal of Solid State Chemistry, 58, 78–86.

Smith, P. P. K. and Parise, J. B. (1985) Structure determination of $SnSb_2S_4$ and $SnSb_2Se_4$ by high-resolution electron microscopy. Acta Crystallographica, B41, 84–87.

Takeda, Hiroshi and Horiuchi, H. (1971) Symbolic addition procedure applied to zinkenite structure determination. Journal of the Mineralogical Society of Japan, 10, 283–295.

Vaux, George and Bannister, F. A. (1938) The identity of zinckenite and keeleyite. Mineralogical Magazine, 25, 221–227.